External Condition-induced Interfacial Charge Transfer in the Single-Walled Carbon Nanotube/Graphene van der Waals Heterostructures

Huan Yin, Ruxuan Zhang, Tian Tian, Zhi Yang, Nantao Hu, Yafei Zhang, and Yanjie Su*[a]

Key Laboratory of Thin Film and Microfabrication (Ministry of Education), Department of Micro/Nano Electronics, School of Electronics, Information and Electrical Engineering, Shanghai Jiao Tong University, Shanghai 200240, PR China

Corresponding author: Yanjie Su, Email: yanjiesu@sjtu.edu.cn

Abstract

Single-walled carbon nanotube (SWCNT)/graphene van der Waals (vdW) heterostructures have shown great potential for use in high-performance carbon-based heterojunction nanodevices owing to their strong interfacial coupling effects and unique physical and chemical properties. However, the interfacial charge transfer process and related influencing factors, which are crucial in determining device performance, have not been adequately investigated. Herein, we systematically investigate the interfacial charge transfer between SWCNTs and graphene using Raman spectroscopy under different external conditions, including bias voltage, temperature, and environmental atmosphere. Our results indicate that electrons are transferred from SWCNTs to graphene when the applied voltage deviates from the neutral point voltage of -4 V. Under various environmental atmospheres and temperature conditions, the built-in electric field induces the electrons transfer from SWCNTs to graphene. Under the humid conditions, electrons are injected into both the SWCNTs and graphene from H_2O molecules. While in an NO_2 atmosphere, holes and electrons are injected into graphene and SWCNTs, respectively, from the NO_2 molecules. Our study not

only provides an important basis for understanding the interfacial charge transfer between SWCNTs and graphene but also provides guidance for designing high-performance all-carbon vdW heterostructure nanodevices.

Keywords: all-carbon heterostructures, interfacial charge transfer, Raman shift, external conditions, bias voltages, environmental atmosphere

Introduction

Carbon allotropes with disparate physical and chemical properties have attracted considerable attention in the field of novel heterostructure nanodevices.[1–3] Specifically, graphene exhibits extraordinary physical and chemical properties, such as an ultrahigh specific surface area, exceptional charge carrier mobility and high thermal conductivity.[4,5] Additionally, semiconducting single-walled carbon nanotubes (SWCNTs) possess a markable aspect ratio, broadband and tunable light absorption, and electronic band structures that depend closely on their chirality and diameter.[6] When SWCNTs and graphene are assembled into all-carbon van der Waals (vdW) heterostructures, they exhibit more fascinating properties compared to their monolithic counterparts, owing to the identical sp^2 hybridization of carbon atoms, well-matched lattice, and strong interfacial coupling.[2,7] The SWCNT/graphene vdW heterostructures have been successfully utilized for fabricating novel photodetectors, humidity sensors, and flexible electronics, [8–14] and are expected achieve even more in the field of nanoelectronics and nano-optoelectronics. SWCNT/graphene vdW heterostructure nanodevices primarily rely on electronic interactions between materials.[15,16] Therefore, understanding the charge transfer mechanism between SWCNTs and graphene is imperative for designing and fabricating all-carbon vdW heterostructure nanodevices with superior performance.

To fully realize the potential of SWCNT/graphene vdW heterostructures, a deeper understanding of the interfacial charge transfer in the heterostructures is

required. To date, only a limited number of studies have investigated charge transfer at the interface between SWCNTs and graphene.[17–21] Peng et al[21] investigated the electronic transport properties of the SWCNT/graphene heterojunctions, and the results suggest that a Schottky barrier exists between the semiconducting SWCNTs and graphene, while no obvious Schottky barrier exists at metallic SWCNT/graphene heterojunctions. Paulus et al.[18] demonstrated that metallic SWCNTs donate electrons to graphene, with a relatively small potential offset between the metallic SWCNTs and graphene. Liu et al.[17] studied the interfacial charge transfer in heterostructures of (6, 5) SWCNTs and graphene using characteristic peak shifts in Raman spectroscopy. Their findings illustrated the transfer of the electrons from metallic SWCNTs to graphene, while holes were transferred from semiconducting SWCNTs to graphene. These studies investigated and summarized the charge-transfer mechanisms at the interface of SWCNT/graphene vdW heterostructures, which are of considerable significance for the study of high-performance nanodevices. However, in addition to the intrinsic interactions between the SWCNTs and graphene, external environmental conditions also change the interfacial charge transfer, thereby influencing the performance of the devices. For example, the environmental temperature of the photodetectors affects their detection ability by influencing the dark current density to some extent. Similarly, for gas sensors based on heterostructures, external conditions such as temperature, humidity, and gas molecule concentration significantly influence the sensing performance.[22–24] However, the effect of external conditions on the interfacial charge transfer in SWCNT/graphene vdW heterostructures is yet to be investigated.

Herein, we systematically investigated the charge transfer process of SWCNT/graphene vdW heterostructures using Raman spectroscopy under different external conditions, including bias voltage, temperature, and environmental atmosphere. The characteristic Raman peaks of the SWCNT/graphene vdW heterostructures exhibited distinct variations under

different conditions, suggesting interfacial charge transfer between the SWCNTs and graphene. Raman spectroscopy has been used to deduce the charge transfer mechanism at the interface of the SWCNT/graphene vdW heterostructures under different conditions. This approach provides a direct support for the design and fabrication of nanodevices. Our results not only provide useful insights into the charge transfer mechanism in SWCNT/graphene vdW heterostructures, but also unveil promising potential applications for all-carbon nanodevices.

Experimental sections

(6,5)-enriched SWCNTs (Sigma-Aldrich, USA, (6,5) chirality, ⩾90% carbon basis) were suspended in N-methyl-2-pyrrolidone (NMP) solution and ultrasonicated for 1 h in an ice water bath for homogenization. To remove the SWCNT bundles, the as-obtained solution was further centrifuged at 12000 rpm for 1h, and the SWCNT networks were formed by spin-coating the supernatant onto SiO_2 (300 nm)/Si. Subsequently, the graphene grown by the chemical vapor deposition (CVD) on a copper foil was transferred on top of the SWCNT networks using the procedures facilitated by poly (methyl methacrylate) (PMMA). The dried sample was immersed in acetone to remove the PMMA. The SWCNT/graphene vdW heterostructures were fabricated after annealed at 120 ℃ for 90 minutes under vacuum conditions. Contrast samples for pure SWCNTs and graphene were prepared in the same manner. Figure 1 shows the schematic of the synthesis procedure.

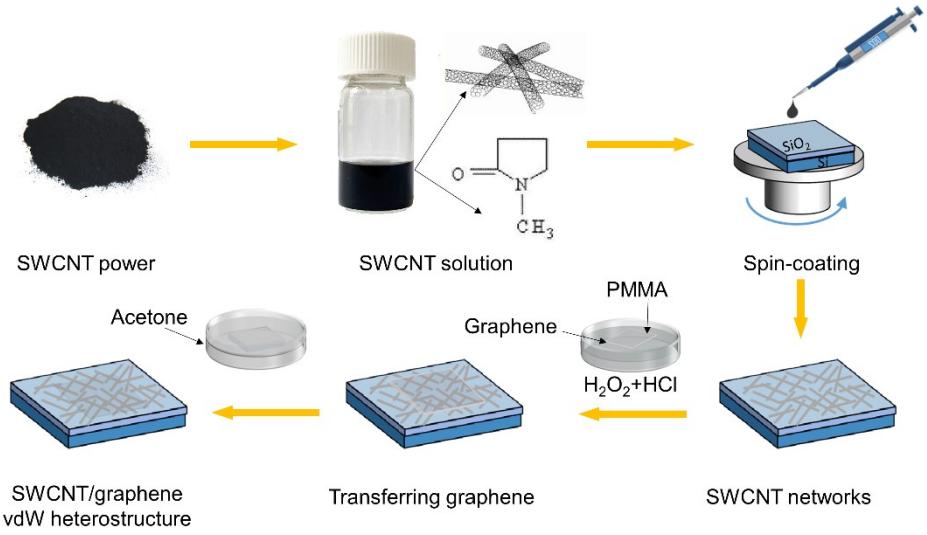

Figure 1 Schematic of the synthesis of the SWCNT/graphene vdW heterostructures.

The micro-morphologies of the SWCNT/graphene vdW heterostructures were observed using scanning electron microscopy (SEM, Zeiss Ultra Plus, Germany). Interfacial charge transfer in the SWCNT/graphene vdW heterostructures was investigated using an inVia Renishaw Raman system with an excitation wavelength of 514 nm. The Raman mapping was performed over a scanning area of approximately 50 × 50 μm^2, containing 100 spectra, with a scanning power of 3 mW and step length of 5 μm using Raman mapping mode. To characterize the effect of the bias voltage on the Raman spectra of the heterostructures, Au electrodes with a thickness of 100 nm were deposited onto the surface of the as-prepared SWCNT/graphene vdW heterostructures. Subsequently, the electrodes were connected to voltage sources at both ends. Raman spectra were collected at various bias voltages. In addition, in-situ Raman characterizations was performed under different relative humidity (RH) conditions by introducing vapors of different humidity into the testing chamber. The desired RH values were achieved by bubbling nitrogen gas through distilled water. Similarly, in-situ Raman characterizations were conducted under an NO_2 gas atmosphere by introducing NO_2 gas with different concentrations into the testing chamber. Furthermore, in-situ Raman characterization was performed

under various temperature conditions by adjusting the substrate temperature within the chamber.

Results and discussion

Figure 2a shows a typical SEM image of the SWCNT/graphene vdW heterostructures. Graphene exhibits numerous folds and breaks at the edges. The SWCNT networks are uniformly distributed on the SiO_2/Si surface. A portion of the SWCNT networks is distributed directly beneath the graphene, resulting in the formation of SWCNT/graphene vdW heterostructures. Raman spectroscopy is a powerful tool for investigating the electronic and structural properties of carbon materials. Figure 2b presents the Raman spectra of the SWCNT/graphene vdW heterostructures, pure SWCNTs, and graphene. The Raman spectrum of graphene exhibits characteristic peaks, including the G (~1589 cm^{-1}) and 2D bands (~2690 cm^{-1}). The D band, which corresponds to disordered vibrations, is commonly used to characterize defects or edges. The absence of the D band indicates high-quality of graphene.[17,25] The 2D band represents a symmetric and sharp Lorentzian feature, indicating single-layer graphene. The characteristic Raman modes of the SWCNTs include the radial breathing mode (RBM) at 100-300 cm^{-1}, D band at ~1586 cm^{-1}, and 2D band at ~2628 cm^{-1}. The G band splits into two bands, namely the G^- (at 1538 cm^{-1}) and G^+ bands (at 1586 cm^{-1}), due to the curvature of the SWCNTs.[26] The diameter of the SWCNTs in our study is estimated based on the RBM positions of the SWCNTs.[27] By analyzing the RBM positions in Figure 2c, we obtained a diameter of ~0.79 nm for the SWCNTs. Moreover, the analysis of charge transfer in SWCNT/graphene vdW heterostructures using the G band is complicated, because the G band of graphene overlaps with that of the SWCNTs. Instead, for the 2D band of the SWCNT/graphene vdW heterostructures (represented by the red curve in Figure 2b), the $2D^-$ and $2D^+$ bands were derived from the partial overlap of the SWCNTs and graphene, respectively.[7] Therefore, the process of interfacial charge transfer in the SWCNT/graphene vdW heterostructures was further analyzed based on changes

in the 2D band. Moreover, only a few data points could not adequately support the Raman spectroscopy results. Consequently, a Raman statistical approach was employed to determine the equilibrium position based on 100 Raman data distributions, thus facilitating a more adequate analysis of the interfacial charge transfer in the heterostructures. This approach allows the evaluation of the position and intensity ratio of 2D band in the SWCNT/graphene vdW heterostructures, providing a more comprehensive analysis of the interfacial charge transfer. 100 high-quality Raman spectra were collected for each sample, and the peak positions and intensities were subsequently analyzed in the form of histograms. A comparison of the G and 2D band positions of the SWCNT/graphene vdW heterostructures, pure SWCNTs, and graphene is shown in Figure 2d-f. Figure 2d shows that the G band of the SWCNT/graphene vdW heterostructures is positioned between the G bands of graphene and that of SWCNTs. Furthermore, there a downshift of approximately 1.6 cm^{-1} is observed in the G band of the SWCNT/graphene vdW heterostructures in comparison to pure graphene. This downshift suggests the doping of graphene by the SWCNT.[18,19] This conclusion is further supported by the G band analysis of the SWCNTs, which suggests the occurrence of charge transfer between graphene and SWCNTs.[7,17] As shown in Figure 2e and 2f, the $2D^{+}$ band of the SWCNT/graphene vdW heterostructures exhibits a shift towards lower frequencies (redshift) when compared to the 2D band of graphene. In contrast, the $2D^{-}$ band experiences a shift towards higher frequencies (blueshift) in comparison to the 2D band of the SWCNTs. These shifts provide evidence for the transfer of electrons from the SWCNTs to graphene. This electron transfer is further supported by the diminished full width at half maximum (FWHM) and 2D/G intensity ratio, as illustrated in Figure S1. Based on the above results, we further investigated the charge transfer in the SWCNT/graphene vdW heterostructures using Raman spectroscopy under various external conditions. To facilitate our analysis, we primarily focused on the trends in the 2D band of

the SWCNT/graphene vdW heterostructures (including the $2D^-$ and $2D^+$ bands) as they change with alterations in the external environment. Trends related to the characteristic peaks of the SWCNTs or graphene in response to external environmental variations have not been addressed individually in this study. Focusing on the study of the 2D band can effectively capture the subtle variations in charge transfer within a specific heterostructure. In addition, this approach avoids the unnecessary complexity associated with analyzing individual SWCNT or graphene components, particularly when studied in different external environments.

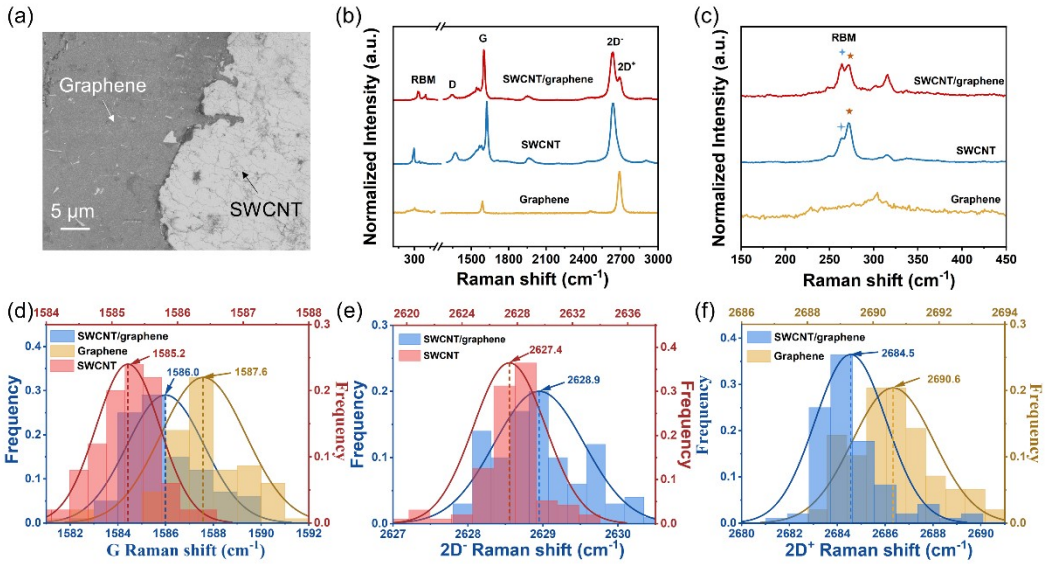

Figure 2 a) SEM image of the SWCNT/graphene vdW heterostructures on the SiO_2/Si substrate. b) Raman spectrum and c) RBM modes of the heterostructures, pure SWCNTs, and graphene. d-f) Histograms of the G, $2D^-$ and $2D^+$ band positions, respectively, in the SWCNT/graphene vdW heterostructures, pure SWCNTs, and graphene.

To investigate the influence of the bias voltage on the charge transfer in the SWCNT/graphene vdW heterostructures, Raman spectra of the heterostructures were obtained at varying bias voltages, as depicted in Figure 3a. As the bias voltage was varied from -10 V to 10 V, noticeable shifts in the position and intensity of $2D^+$ and $2D^-$ bands within the heterostructures were observed,

indicating the significant influence of the bias voltage on the charge transfer behavior. The Raman statistical results are shown in Figure 3b-e. Figure 3b illustrates the behavior of the $2D^-$ band in the heterostructures as a function of bias voltage. When a bias of -4 V is applied, the position of the $2D^-$ band approaches the position of the 2D band in pure SWCNTs. At this point, a -4 V bias is established as the neutrality point. In Figure 3b, when the bias voltage is below -4 V, the $2D^-$ band exhibits varying degrees of blueshift. Notably, the larger the negative bias applied, the greater is the blueshift of the $2D^-$ band. This indicates that the hole-doping effect in the SWCNT increased with an increase in the reverse voltage. At this point, the holes were transferred from the graphene to the SWCNTs. Similarly, when the applied voltage exceeds -4 V, the $2D^-$ band also shows varying degrees of blueshift. As the applied voltage deviates further from the neutrality point of -4 V, the blueshift of the $2D^-$ band increases, indicating a greater transfer of holes from graphene to SWCNTs. The charge transfer in the SWCNT/graphene vdW heterostructures was also evaluated by analyzing the $2D^+$ band, as illustrated in Figure 3c, which provides information about the doping of graphene.[17] Despite exhibiting opposite behaviors, an analysis of both the $2D^+$ and $2D^-$ bands leads to the same conclusion regarding charge transfer. Specifically, at a bias voltage of -4 V, the position of the $2D^+$ band closely aligns with the position of the 2D band in pure graphene. This suggests that the Fermi energy level of graphene in the heterostructures precisely matches the Dirac point at this bias voltage. The position of the $2D^+$ band reaches a neutral point at a bias voltage of -4 V, and the deviation of the applied voltage from the neutrality point results in varying degrees of redshift. This suggests that graphene is electron-doped for voltages other than -4 V, indicating the electron transfer from SWCNTs to graphene. In addition, the intensity ratios of $2D^+/G$ and $2D^+/2D^-$ also exhibited variations with the bias voltage, as shown in Figure 3d and 3e, respectively. Both the $2D^+/G$ and $2D^+/2D^-$ intensity ratios provide further information on graphene doping. The behavior of the $2D^+/G$ intensity ratios is

generally consistent with that of the $2D^+/2D^-$ intensity ratios, confirming the occurrence of charge transfer between the SWCNTs and graphene at different voltages. Combined with the above results, we propose energy-band diagrams (Figure 3f) to illustrate the energy-band alignment in the SWCNT/graphene vdW heterostructures under different bias voltages. At a bias voltage of -4 V, the positions of the $2D^-$ and $2D^+$ bands align with those of pure SWCNTs and graphene, respectively, indicating the absence of further charge transfer between the SWCNTs and graphene. Therefore, a bias voltage of -4 V is considered as a neutral point. When the applied voltage deviates from the neutral-point voltage, the electrons are transferred from the SWCNTs to the graphene. Therefore, applying a bias voltage to the SWCNT/graphene vdW heterostructures facilitates the transfer of electrons from SWCNTs to graphene.

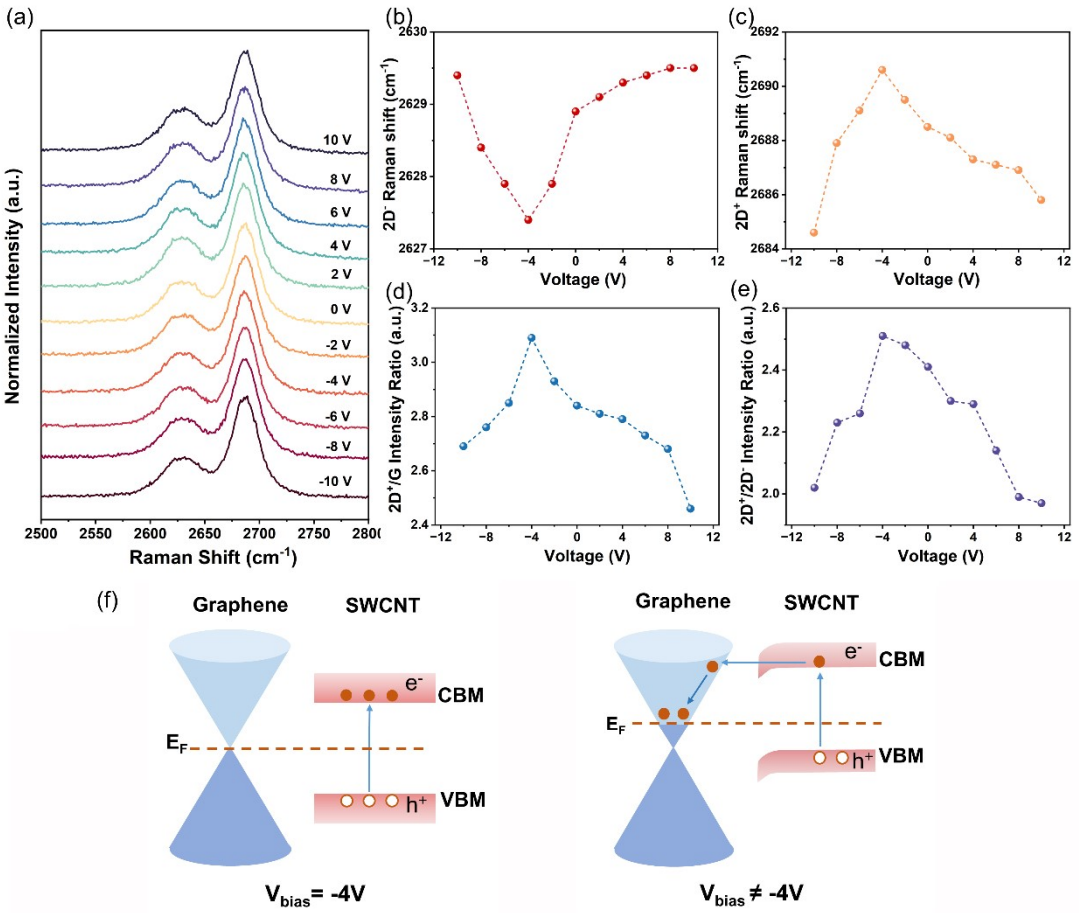

Figure 3 a) Raman spectra of theSWCNT/graphene vdW heterostructures at various bias voltages. b) $2D^-$ band, c) $2D^+$ band, d) $2D^+/G$ intensity ratio, and e) $2D^+/2D^-$ intensity ratio with

respect to the bias voltage. f) Energy band diagram of the SWCNT/graphene vdW heterostructures with different bias voltages.

Humidity is an important parameter of the environmental atmosphere that influences nanodevice performance through interactions between H_2O molecules and nanomaterials.[28,29] In this study, we additionally investigated the interactions and related charge transfer processes between H_2O molecules and SWCNT/graphene vdW heterostructures using Raman spectroscopy. Figure 4a depicts the variation in the 2D band of the SWCNT/graphene vdW heterostructures as a function of RH ranging from 0 to 80%. The responses of the $2D^-$ and $2D^+$ bands to varying RHs were fitted and are presented in Figure 4b-e. An exponential relationship has been established between the peak position and RH, with R^2 >0.93 for each sample by fitting the curve using the function: $y = A_1 e^{-x/t_1} + A_2 e^{-x/t_2} + y_0$, where y corresponds to the position (cm^{-1}) of the $2D^-$ and $2D^+$ bands, x represents the RH, and A_1, A_2, t_1, and t_2 are parameters obtained from the fitting, respectively. Obviously, Raman shifts to lower frequencies were observed in both the $2D^-$ and $2D^+$ bands in the SWCNT/graphene vdW with an increase in the RH. This phenomenon can be attributed to the gradual adsorption of the H_2O molecules onto the surfaces of the heterostructures. The observed redshift in both the $2D^-$ and $2D^+$ bands indicates the transfer of electrons from H_2O to SWCNTs and graphene.[30,31] The $2D^+$ band exhibits a greater redshift in comparison to the $2D^-$ band, illustrating that the doped electrons in graphene originate not only from the SWCNTs but also from the H_2O molecules.[24] This suggests that H_2O molecules facilitate the transfer of electrons in the SWCNT/graphene vdW heterostructures. Figure 4d further supports the occurrence of electron doping in graphene, as evidenced by the reduction in the $2D^+$/G intensity ratio with increasing RH. Furthermore, the data in Figure 4e indicate that the $2D^+/2D^-$ intensity ratio ($I_{graphene}/I_{SWCNT}$) of the SWCNT/graphene vdW heterostructures increased as the RH increased from 0% to 80%. This trend suggests a better enhancement of the electron doping effect in graphene than in the SWCNTs.[17,24] This observation further supports the notion that the presence of H_2O molecules

contributes to the processes of electron transfer and doping within the heterostructures. Figure 4f illustrates the energy band diagram and a schematic of the SWCNT/graphene vdW heterostructures that are influenced by the adsorption of H_2O molecules. It can be observed that H_2O molecules are adsorbed on the surface of SWCNTs, facilitating the transfer of electrons from these molecules to the SWCNTs. Additionally, the SWCNT/graphene vdW heterostructures facilitate the transfer of a fraction of the injected electrons from the SWCNTs to graphene.[24] Nevertheless, some of the injected electrons are unable to transfer promptly, resulting in the redshift of the $2D^-$ band. The behavior of the $2D^-$ band indicates that a higher quantity of electrons is transferred from the H_2O molecules to the SWCNTs, as the RH increases. In addition to receiving electrons from the SWCNTs, graphene also demonstrates the ability to extract electrons from H_2O molecules. This was supported by the Raman statistical results for pure graphene at different RHs values (Figure S2). As a result, under humid conditions, H_2O molecules inject electrons into both the SWCNTs and graphene. More importantly, the presence of SWCNT/graphene vdW heterostructures facilitated the transfer of a fraction of these injected electrons from the SWCNTs to graphene. This result indicates that fluctuations in humidity in the external environment can affect the interfacial charge transfer in SWCNT/graphene heterostructures, which makes these heterostructures promising candidates for use in humidity sensors.

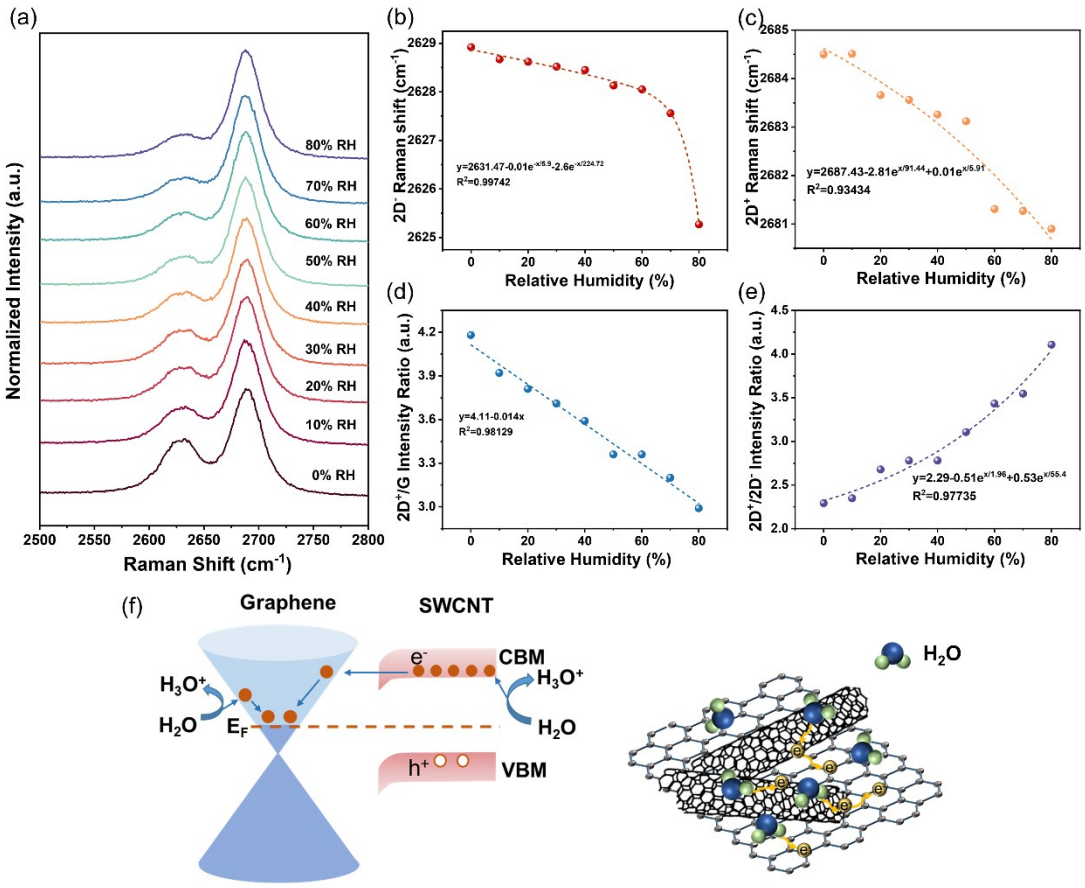

Figure 4 a) The 2D band of SWCNT/graphene vdW heterostructures at various humidity, b) $2D^-$ band, c) $2D^+$ band, d) $2D^+/G$ intensity ratio and e) $2D^+/2D^-$ intensity ratio with respect to different RHs. f) Energy band diagram and schematic of the SWCNT/graphene vdW heterostructures with H_2O molecules. The H_2O molecules are not acting as reducing agent/oxidant, they are solely used to represent components of the electron transfer pathway. The dashed curves and equations in the figures are exponential-fitting results. R^2 indicates the coefficient of determination.

In addition to H_2O molecules, the charge transfer process between other gas molecules and the SWCNT/graphene vdW heterostructures at room temperature was systematically investigated. NO_2 gas, which is typical toxic gas, was selected for this study. Figure 5a shows the alteration of the 2D band in response to various concentrations of NO_2, demonstrating the Raman shift trends of the $2D^-$ and $2D^+$ bands at NO_2 gas concentrations ranging from 0 to 500 ppm. These findings clearly indicate that an increase in NO_2 concentration leads to a successive

redshift of the $2D^-$ band and a continuous blueshift of the $2D^+$ band, as shown in Figures 5b and 5c, respectively. This phenomenon suggests that when NO_2 molecules adhere onto the surface of the SWCNT/graphene vdW heterostructures, the SWCNTs extract electrons from the NO_2 molecules, whereas graphene injects the electrons into the NO_2 molecules.[23,32] The electrons extracted from the NO_2 molecules by the SWCNTs are subsequently transferred to graphene, resulting in a redshift in the $2D^-$ band. However, the number of electrons transferred from NO_2 to the SWCNTs significantly surpassed the number of electrons extracted from graphene by the NO_2 molecules. Consequently, the $2D^+$ band experienced a blueshift with increasing NO_2 concentration. Notably, the $2D^+/G$ intensity ratio serves as a sensitive indicator for monitoring graphene doping. A decrease in the $2D^+/G$ value was observed after the adsorption of NO_2 molecules (Figure 5d), indicating graphene doping. However, these changes were the same for both electron and hole dopings.[33,34] Moreover, as shown in Figure 5e, the $2D^+/2D^-$ intensity ratio of the SWCNT/graphene vdW heterostructures decreased as the concentration of NO_2 increased from 0 to 500 ppm. This decline can be attributed to a reduction in the hole doping in graphene.[7] This trend is further accentuated at higher concentrations of NO_2 molecules, where the adsorption sites on graphene become saturated, leading to a gradual alteration in the Raman peak positions and intensity. Consequently, this saturation effect ultimately leads to a plateau in the response of the heterostructures to varying NO_2 concentrations.[35] An exponential relationship exists between the positions of the $2D^-$ band, $2D^+$ band, $2D^+/G$ intensity ratio, and $2D^+/2D^-$ intensity ratio and NO_2 concentrations. These fitted curves of the related trends can be expressed by the following equation: $y = A_1 e^{-x/t_1} + A_2 e^{-x/t_2} + y_0$, where y corresponds to the $2D^-$ band position, $2D^+$ band position, $2D^+/G$ intensity ratio, and $2D^+/2D^-$ intensity ratio; x represents the NO_2 gas concentrations; A_1, A_2, t_1 and t_2 are the parameters obtained from the fitting; and y_0 represents the baseline or offset. These parameters are presented in the corresponding figures. Moreover, high R^2 values, greater than 0.98, indicate strong agreement between the fitted curves and experimental

data, as shown in Figure 5b-e. According to the above analysis, the interfacial charge transfer in SWCNT/graphene vdW heterostructures can be evaluated when exposed to varying concentrations of NO_2 gas. Figure 5f illustrates the energy-band diagram and schematic of the SWCNT/graphene vdW heterostructures, which were predicated based on the interactions between the NO_2 molecules and the heterostructures. Upon the adherence of the NO_2 molecules onto the surface of the heterostructures, electrons are transferred from the NO_2 molecules to the SWCNTs, resulting in a remarkable increase in electrons in SWCNTs. However, the holes are trapped in the SWCNTs because of potential barrier at the heterostructures interface.[13,24] Moreover, the heterostructures promote the transfer of some of the electrons injected by NO_2 molecules from the SWCNTs to graphene, owing to the presence of a built-in electric field.[36] However, the NO_2 molecules extract a large number of electrons from graphene, significantly exceeding the number extracted from the SWCNTs, resulting in a significant increase in the number of holes in graphene. This observation implies that changes in the concentration of specific gas molecules can also affect the interfacial charge transfer of SWCNT/graphene heterostructures, which provides a novel method for gas detection.

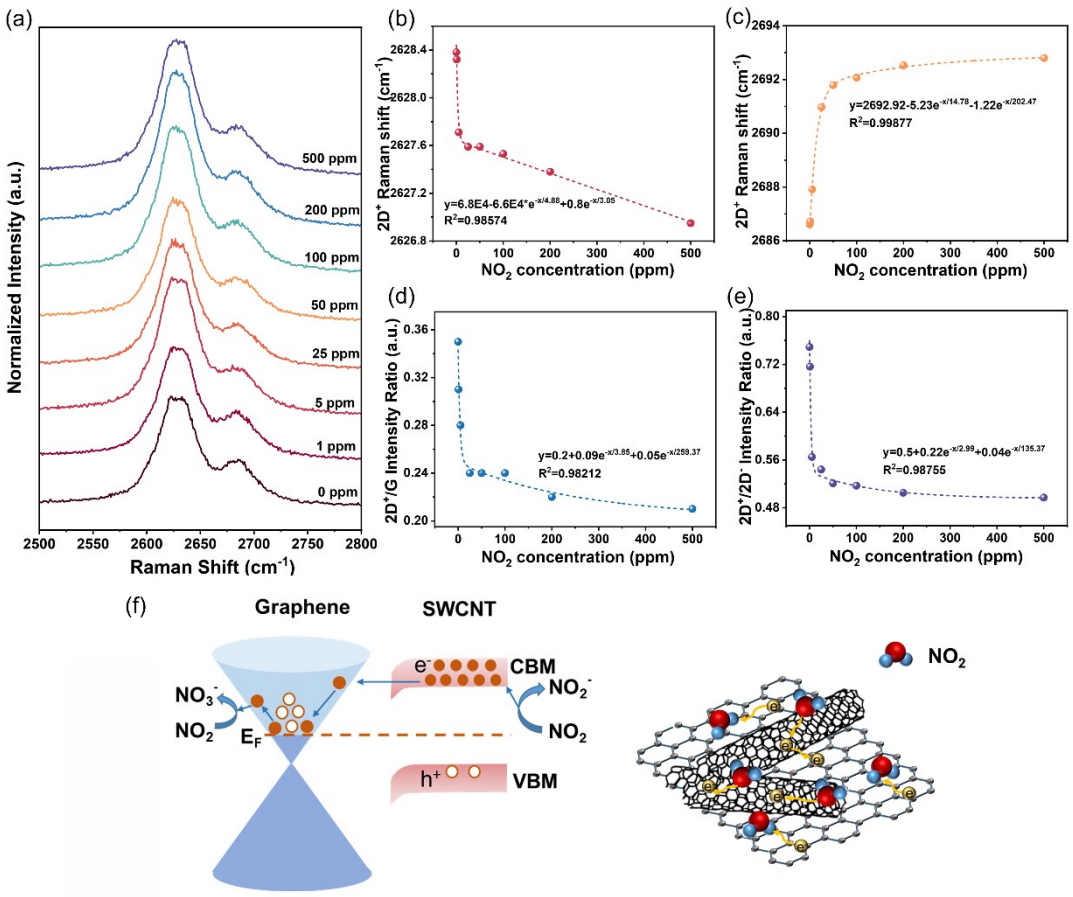

Figure 5 a) The 2D band of the SWCNT/graphene vdW heterostructures at various NO_2 gas concentrations, b) $2D^-$ band, c)$2D^+$ band, d) $2D^+/G$ intensity ratio, and e)$2D^+/2D^-$ intensity ratio as functions of different NO_2 gas concentrations. f) Energy band diagram and schematic of the SWCNT/graphene vdW heterostructures with NO_2 molecules. The NO_2 molecules are not acting as reducing agent/oxidant; they are solely used to represent the components of the electron transfer pathway. The dashed curves and equations in the figures are exponential-fitting results. R^2 indicates the coefficient of determination.

Raman spectroscopy was employed to investigate the temperature-dependent characteristics of the $2D^-$ and $2D^+$ bands in the SWCNT/graphene vdW heterostructures. Raman spectra of the heterostructure samples were measured in the temperature range of 295-473 k. Figure 6a illustrates significant changes in the position and intensity of the $2D^-$ and $2D^+$ bands with temperature, indicating the temperature-dependent behavior of the heterostructures. A data analysis revealed a consistent linear correlation between the $2D^-$ and $2D^+$ band

positions, as well as the $2D^+/2D^-$ intensity ratio, with temperature, as shown in Figure 6b-d. The results demonstrate that the $2D^-$ and $2D^+$ bands red-shift with increasing temperature, whereas the intensity ratio of $2D^+/G$ decreases with increasing temperature. These temperature-dependent behaviors suggest changes in the electronic structure and doping effects of the SWCNT/graphene vdW heterostructures under different temperature conditions. The dashed lines in Figure 6b-d were fitted by $y = a + bT$, where y corresponds to the $2D^-$ band position, $2D^+$ band position, and $2D^+/G$ intensity ratio; T represents the temperature; and a and b are the parameters obtained from the fitting. These linear relationships resemble the temperature dependence previously reported for the Raman spectra of pure SWCNTs and graphene.[37,38] However, the fitted slopes and intercepts obtained in our investigation are comparatively larger, and these can be attributed to the interfacial charge transfer in the heterostructures. This charge transfer can be detected by the 2D Raman band shift of the heterostructures. Notably, the fitted slopes indicate that the $2D^+$ band experienced a more significant redshift than the $2D^-$ band, indicating the transfer of some electrons from the SWCNTs to graphene. Furthermore, the decrease in the $2D^+/G$ intensity ratio supports the view that charge transfer at the heterostructure interfaces increases with increasing temperature. Figure 6e shows that graphene exhibits a higher number of defects at elevated temperatures, resulting in an alteration in the trend of the $2D^+/2D^-$ intensity ratio. Consequently, we do not discuss the $2D^+/2D^-$ intensity ratio further because the Raman spectra were obtained under ambient conditions. Although the data obtained under vacuum conditions offer greater precision, our results still offer preliminary insights into the correlation between interfacial charge transfer and temperature. In summary, the statistical analysis of the changes in the characteristic Raman peaks serves as an effective method for deducing the charge transfer at the interface of the SWCNT/graphene heterostructures (Table S1).

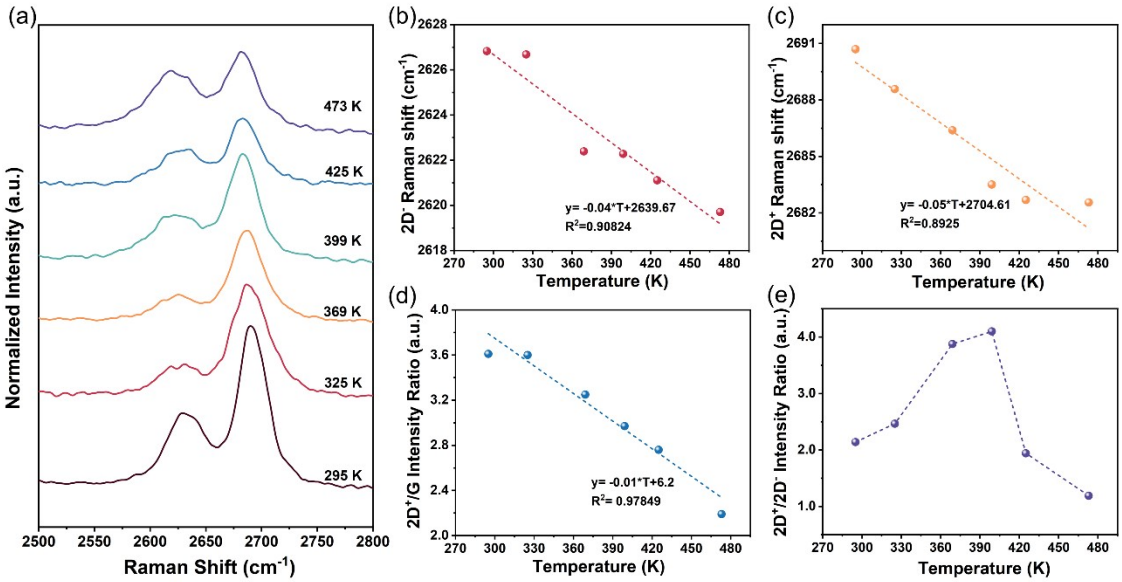

Figure 6 a) The SWCNT/graphene vdW heterostructures at various temperatures, the temperature dependence of b) $2D^-$ band, c) $2D^+$ band, d) $2D^+/G$ intensity ratio and e) $2D^+/2D^-$ intensity ratio, respectively. The dashed curves and the equations in the figures are exponential-fitting results. R^2 indicates the coefficient of determination.

Conclusion

In summary, we explored the interfacial charge transfer mechanism of SWCNT/graphene vdW heterostructures under different conditions using Raman spectroscopy. The interfacial charge transfer process between the SWCNTs and graphene was demonstrated by analyzing the characteristic peaks observed in the heterostructures under different conditions. The bias voltage applied to the SWCNT/graphene vdW heterostructures caused corresponding changes in the Fermi levels of graphene. No charge transfer was observed between the SWCNTs and graphene at a bias voltage of -4 V. For applied voltages below or above -4 V, the electrons were transferred from the SWCNTs to graphene. Under various atmospheric and temperature conditions, the built-in electric field of the SWCNT/graphene vdW heterostructures induced partial electron transfer from the SWCNTs to graphene. Moreover, the charge transfer mechanisms in heterostructures vary under different environmental atmospheres. Under humid

conditions, H_2O molecules inject electrons into both SWCNTs and graphene. Under NO_2 gas conditions, the NO_2 molecules inject the holes and electrons into graphene and SWCNTs, respectively. These results demonstrate that the performance of the SWCNT/graphene heterostructure nanodevices is influenced by various external conditions. This study not only provides a useful basis for the mechanism of interfacial charge transfer in SWCNT/graphene vdW heterostructures but also expands the potential applications of all-carbon heterojunction detectors.

Supporting Information.

2D band of pure graphene as tend of different RHs. The histograms of $2D^+/G$ intensity ratio and the FWHM of $2D^+$ band in the SWCNT/graphene vdW heterostructures, and pure graphene. The charge transfer at the interfaces under different external conditions.

Acknowledgments

The authors gratefully acknowledge financial support from the National Natural Science Foundation of China (Nos. 61974089 and 62171275) and the Oceanic Interdisciplinary Program of Shanghai Jiao Tong University (SL2020MS001). The authors also acknowledge the analysis support from the Instrumental Analysis Center of SJTU and the Center for Advanced Electronic Materials and Devices of SJTU.

References

(1) Lv, R.; Cruz-Silva, E.; Terrones, M. Building Complex Hybrid Carbon Architectures by Covalent Interconnections: Graphene-Nanotube Hybrids and More. *ACS Nano* **2014**, *8* (5), 4061–4069. https://doi.org/10.1021/nn502426c.

(2) Liu, Y.; Wang, F.; Wang, X.; Wang, X.; Flahaut, E.; Liu, X.; Li, Y.; Wang, X.; Xu, Y.; Shi, Y.; Zhang, R. Planar Carbon Nanotube–Graphene Hybrid Films for High-Performance Broadband Photodetectors. *Nat. Commun.* **2015**, *6* (1), 8589. https://doi.org/10.1038/ncomms9589.

(3) Song, P.; Yang, J.; Wang, C.; Wang, T.; Gao, H.; Wang, G.; Li, J. Interface Engineering of Fe_7S_8/FeS_2 Heterostructure in Situ Encapsulated into Nitrogen-Doped Carbon Nanotubes for High Power Sodium-Ion Batteries. *NANO-MICRO Lett.* **2023**, *15* (1), 118. https://doi.org/10.1007/s40820-023-01082-w.

(4) Feng, W.; Long, P.; Feng, Y.; Li, Y. Two-Dimensional Fluorinated Graphene: Synthesis, Structures, Properties and Applications. *Adv. Sci.* **2016**, *3* (7), 1500413. https://doi.org/10.1002/advs.201500413.

(5) Zarepour, A.; Ahmadi, S.; Rabiee, N.; Zarrabi, A.; Iravani, S. Self-Healing MXene- and Graphene-Based Composites: Properties and Applications. *NANO-MICRO Lett.* **2023**, *15* (1), 100. https://doi.org/10.1007/s40820-023-01074-w.

(6) Cai, X.; Wang, S.; Peng, L. M. Recent Progress of Photodetector Based on Carbon Nanotube Film and Application in Optoelectronic Integration. *Nano Res. Energy* **2023**. https://doi.org/10.26599/NRE.2023.9120058.

(7) Cai, B.; Su, Y.; Tao, Z.; Hu, J.; Zou, C.; Yang, Z.; Zhang, Y. Highly Sensitive Broadband Single-Walled Carbon Nanotube Photodetectors Enhanced by Separated Graphene Nanosheets. *Adv. Opt. Mater.* **2018**, *6* (23), 1800791. https://doi.org/10.1002/adom.201800791.

(8) Kim, S. H.; Song, W.; Jung, M. W.; Kang, M. A.; Kim, K.; Chang, S. J.; Lee, S. S.; Lim, J.; Hwang, J.; Myung, S.; An, K.-S. Carbon Nanotube and Graphene Hybrid Thin Film for Transparent Electrodes and Field Effect Transistors. *Adv. Mater.* **2014**, *26* (25), 4247–4252. https://doi.org/10.1002/adma.201400463.

(9) Cheng, Q.; Tang, J.; Ma, J.; Zhang, H.; Shinya, N.; Qin, L. C. Graphene and Carbon Nanotube Composite Electrodes for Supercapacitors with Ultra-High Energy Density. *Phys. Chem. Chem. Phys.* **2011**, *13* (39), 17615–17624. https://doi.org/10.1039/C1CP21910C.

(10) Zhao, M.-Q.; Liu, X.-F.; Zhang, Q.; Tian, G. L.; Huang, J. Q.; Zhu, W.; Wei, F. Graphene/Single-Walled Carbon Nanotube Hybrids: One-Step Catalytic Growth and Applications for High-Rate Li–S Batteries. *ACS Nano* **2012**, *6* (12), 10759–10769. https://doi.org/10.1021/nn304037d.

(11) Chae, S. H.; Lee, Y. H. Carbon Nanotubes and Graphene towards Soft Electronics. *Nano Converg.* **2014**, *1* (1), 15. https://doi.org/10.1186/s40580-014-0015-5.

(12) Liu, Y.; Shen, Y.; Sun, L.; Li, J.; Liu, C.; Ren, W.; Li, F.; Gao, L.; Chen, J.; Liu, F.; Sun, Y.; Tang, N.; Cheng, H.-M.; Du, Y. Elemental Superdoping of Graphene and Carbon Nanotubes. *Nat. Commun.* **2016**, *7* (1), 10921. https://doi.org/10.1038/ncomms10921.

(13) Zhang, Y.; Li, Y.; You, Q.; Sun, J.; Li, K.; Hong, H.; Kong, L.; Zhu, M.; Deng, T.; Liu, Z. A Broadband 3D Microtubular Photodetector Based on a Single Wall Carbon Nanotube–Graphene Heterojunction. *Nanoscale* **2023**, *15* (3), 1402–1411. https://doi.org/10.1039/D2NR05819G.

(14) Zhang, Y.; Deng, T.; Li, S.; Sun, J.; Yin, W.; Fang, Y.; Liu, Z. Highly Sensitive Ultraviolet Photodetectors Based on Single Wall Carbon Nanotube-Graphene Hybrid Films. *Appl. Surf. Sci.* **2020**, *512*, 145651. https://doi.org/10.1016/j.apsusc.2020.145651.

(15) Luo, D.; Tang, J.; Shen, X.; Ji, F.; Yang, J.; Weathersby, S.; Kozina, M. E.; Chen, Z.; Xiao, J.; Ye, Y.; Cao, T.; Zhang, G.; Wang, X.; Lindenberg, A. M. Twist-Angle-Dependent Ultrafast Charge Transfer in MoS2-Graphene van Der Waals Heterostructures. *Nano Lett.* **2021**, *21* (19), 8051–8057. https://doi.org/10.1021/acs.nanolett.1c02356.

(16) Yin, Y.; Zhao, X.; Ren, X.; Liu, K.; Zhao, J.; Zhang, L.; Li, S. Thickness Dependent Ultrafast Charge Transfer in BP/MoS2 Heterostructure. *Adv. Funct. Mater.* **2022**, *32* (45), 2206952. https://doi.org/10.1002/adfm.202206952.

(17) Liu, Y.; Wang, F.; Liu, Y.; Wang, X.; Xu, Y.; Zhang, R. Charge Transfer at Carbon Nanotube–Graphene van Der Waals Heterojunctions. *Nanoscale* **2016**, *8* (26), 12883–12886. https://doi.org/10.1039/C6NR03965K.

(18) Paulus, G. L. C.; Wang, Q. H.; Ulissi, Z. W.; McNicholas, T. P.; Vijayaraghavan, A.; Shih, C.-J.; Jin, Z.; Strano, M. S. Charge Transfer at Junctions of a Single Layer of Graphene and a Metallic Single Walled Carbon Nanotube. *Small* **2013**, *9* (11), 1954–1963. https://doi.org/10.1002/smll.201201034.

(19) Rao, R.; Pierce, N.; Dasgupta, A. On the Charge Transfer between Single-Walled Carbon Nanotubes and Graphene. *Appl. Phys. Lett.* **2014**, *105* (7), 073115. https://doi.org/10.1063/1.4893698.

(20) Rao, C. N. R.; Voggu, R. Charge-Transfer with Graphene and Nanotubes. *Mater. Today* **2010**, *13* (9), 34–40. https://doi.org/10.1016/S1369-7021(10)70163-2.

(21) Pei, T.; Xu, H.; Zhang, Z.; Wang, Z.; Liu, Y.; Li, Y.; Wang, S.; Peng, L. M. Electronic Transport in Single-Walled Carbon Nanotube/Graphene Junction. *Appl. Phys. Lett.* **2011**, *99* (11), 113102. https://doi.org/10.1063/1.3636407.

(22) Brohmann, M.; Rother, M.; Schießl, S. P.; Preis, E.; Allard, S.; Scherf, U.; Zaumseil, J. Temperature-Dependent Charge Transport in Polymer-Sorted Semiconducting Carbon Nanotube Networks with Different Diameter Distributions. *J. Phys. Chem. C* **2018**, *122* (34), 19886–19896. https://doi.org/10.1021/acs.jpcc.8b04302.

(23) Tian, T.; Yin, H.; Zhang, L.; Zhu, M.; Ma, D.; Shao, F.; Hu, N.; Yang, Z.; Zhang, Y.; Su, Y. Gas Sensing Performance and Charge-Transfer Mechanism of

Semiconducting Single-Walled Carbon Nanotubes. *Appl. Surf. Sci.* **2023**, *609*, 155357. https://doi.org/10.1016/j.apsusc.2022.155357.

(24) Cai, B.; Yin, H.; Huo, T.; Ma, J.; Di, Z.; Li, M.; Hu, N.; Yang, Z.; Zhang, Y.; Su, Y. Semiconducting Single-Walled Carbon Nanotube/Graphene van Der Waals Junctions for Highly Sensitive All-Carbon Hybrid Humidity Sensors. *J. Mater. Chem. C* **2020**, *8* (10), 3386–3394. https://doi.org/10.1039/C9TC06586E.

(25) Tabassian, R.; Nguyen, V. H.; Umrao, S.; Mahato, M.; Kim, J.; Porfiri, M.; Oh, I. Graphene Mesh for Self-Sensing Ionic Soft Actuator Inspired from Mechanoreceptors in Human Body. *Adv. Sci.* **2019**, *6* (23), 1901711. https://doi.org/10.1002/advs.201901711.

(26) Kukovecz, A.; Kramberger, Ch.; Georgakilas, V.; Prato, M.; Kuzmany, H. A Detailed Raman Study on Thin Single-Wall Carbon Nanotubes Prepared by the HiPCO Process. *Eur. Phys. J. B* **2002**, *28* (2), 223–230. https://doi.org/10.1140/epjb/e2002-00224-8.

(27) Abozied, A. M.; Abouelsayed, A.; Hassan, A. F.; Ramadan, A. A.; Al-Ashkar, E. A.; Anis, B. Optical and Electronic Properties of Iodine and Bromine Doped Chirality Enriched (12,1) and (13,2) Single-Walled Carbon Nanotubes. *Carbon* **2021**, *185*, 578–590. https://doi.org/10.1016/j.carbon.2021.09.056.

(28) Zhang, L.; Tan, Q.; Wang, Y.; Fan, Z.; Lin, L.; Zhang, W.; Xiong, J. Wirelessly Powered Multi-Functional Wearable Humidity Sensor Based on RGO-WS2 Heterojunctions. *Sens. Actuators B Chem.* **2021**, *329*, 129077. https://doi.org/10.1016/j.snb.2020.129077.

(29) Lu, L.; Jiang, C.; Hu, G.; Liu, J.; Yang, B. Flexible Noncontact Sensing for Human–Machine Interaction. *Adv. Mater.* **2021**, *33* (16), 2100218. https://doi.org/10.1002/adma.202100218.

(30) Wroblewska, A.; Gordeev, G.; Duzynska, A.; Reich, S.; Zdrojek, M. Doping and Plasmonic Raman Enhancement in Hybrid Single Walled Carbon Nanotubes Films with Embedded Gold Nanoparticles. *Carbon* **2021**, *179*, 531–540. https://doi.org/10.1016/j.carbon.2021.04.079.

(31) Iyengar, S. A.; Srikrishnarka, P.; Jana, S. K.; Islam, M. R.; Ahuja, T.; Mohanty, J. S.; Pradeep, T. Surface-Treated Nanofibers as High Current Yielding Breath Humidity Sensors for Wearable Electronics. *ACS Appl. Electron. Mater.* **2019**, *1* (6), 951–960. https://doi.org/10.1021/acsaelm.9b00123.

(32) Srivastava, S.; Pal, P.; Sharma, D. K.; Kumar, S.; Senguttuvan, T. D.; Gupta, B. K. Ultrasensitive Boron–Nitrogen-Codoped CVD Graphene-Derived NO2 Gas Sensor. *ACS Mater. Au* **2022**, *2* (3), 356–366. https://doi.org/10.1021/acsmaterialsau.2c00003.

(33) Naumenko, D.; Snitka, V.; Snopok, B.; Arpiainen, S.; Lipsanen, H. Graphene-Enhanced Raman Imaging of TiO2 Nanoparticles. *Nanotechnology* **2012**, *23* (46), 465703. https://doi.org/10.1088/0957-4484/23/46/465703.

(34) Das, B.; Voggu, R.; Sekhar Rout, C.; R. Rao, C. N. Changes in the Electronic Structure and Properties of Graphene Induced by Molecular Charge-Transfer. *Chem. Commun.* **2008**, *0* (41), 5155–5157. https://doi.org/10.1039/B808955H.

(35) Guo, X.; Zhang, Y.; Peng, Y. Polyethylenimine-Grafted Graphene Oxide: A Versatile Photothermal Nanocomposite for Catalysis and Carbon Dioxide Capture-and-Release under Simulated and Natural Sunlight. *Monatshefte Für Chem. - Chem. Mon.* **2023**, *154* (3), 367–377. https://doi.org/10.1007/s00706-023-03055-6.

(36) Dariyal, P.; Sharma, S.; Singh Chauhan, G.; Pratap Singh, B.; R. Dhakate, S. Recent Trends in Gas Sensing via Carbon Nanomaterials: Outlook and Challenges. *Nanoscale Adv.* **2021**, *3* (23), 6514–6544. https://doi.org/10.1039/D1NA00707F.

(37) Li, H. D.; Yue, K. T.; Lian, Z. L.; Zhan, Y.; Zhou, L. X.; Zhang, S. L.; Shi, Z. J.; Gu, Z. N.; Liu, B. B.; Yang, R. S.; Yang, H. B.; Zou, G. T.; Zhang, Y.; Iijima, S.

Temperature Dependence of the Raman Spectra of Single-Wall Carbon Nanotubes. *Appl. Phys. Lett.* **2000**, *76* (15), 2053–2055. https://doi.org/10.1063/1.126252.

(38) Calizo, I.; Miao, F.; Bao, W.; Lau, C. N.; Balandin, A. A. Variable Temperature Raman Microscopy as a Nanometrology Tool for Graphene Layers and Graphene-Based Devices. *Appl. Phys. Lett.* **2007**, *91* (7), 071913. https://doi.org/10.1063/1.2771379.